Journal of Electronics and Electrical Engineering
https://ojs.wiserpub.com/index.php/JEEE/

Article

CNN-Based Tree Classification Using Multiwavelength Airborne Polarimetric LiDAR Data

Zhong Hu [1], Songxin Tan [2,*]

[1] Department of Mechanical Engineering, J.J. Lohr College of Engineering, South Dakota State University, Brookings, SD 57007, USA

[2] Department of Electrical Engineering and Computer Science, J.J. Lohr College of Engineering, South Dakota State University, Brookings, SD 57007, USA

E-mail: songxin.tan@sdstate.edu

Received: 3 April 2025; **Revised:** 20 May 2025; **Accepted:** 18 June 2025

Abstract: LiDAR as a commonly used active remote sensing method has been frequently applied in fields like forestry and agriculture. Many existing studies have utilized commercial non-polarimetric LiDAR for vegetation surveying and monitoring. A multiwavelength airborne polarimetric LiDAR system (MAPL) was developed for vegetation remote sensing. The MAPL has dual-wavelength (1063-nm and 532-nm), dual-polarization (co- and cross-polarization), and full waveform recording, and hence leverages enhanced capabilities for target identification and classification. In this work, the MAPL data from five different tree types, blue spruce, ponderosa pine, Austrian pine, ash and maple, were collected. A convolutional neural network (CNN) approach was adopted to classify the trees. The numerical features, i.e., the peak reflectance intensities and the full width at half maxima (FWHMs), were extracted from the MAPL waveforms as input to the CNN model. Four different scenarios were studied, i.e., SCENARIO 1, dual-wavelength and dual-polarization; SCENARIO 2, single wavelength at 1064-nm with dual-polarization; SCENARIO 3, single wavelength at 532-nm with dual-polarization; and SCENARIO 4, dual-wavelength with co-polarization only. The study reveals that as the number of the CNN hidden layers increases, the tree-classification accuracy also improves following a logistic growth model. Furthermore, when the number of hidden layers is greater than 5, SCENARIO 1 has the highest stability (minimum deviation) and the fastest convergence. The results indicate that both the peak intensity and FWHMs of the MAPL waveforms are potent features for deep learning to classify trees, and CNN is an effective tree classification method in this case. The methodology can be extended to other agricultural and forestry remote sensing applications.

Keywords: remote sensing, LiDAR, polarization, full waveform, vegetation classification, convolutional neural network

1. Introduction

Climate change has significant and direct impacts on both agriculture and forestry, so monitoring practices in these sectors are critical to the understanding of and responding to the changing conditions. This includes tracking changes in crop yields, tree health, and ecosystem resilience due to shifting in weather patterns such as extreme heat, droughts, and floods. It necessitates continuous monitoring to adjust and reduce the effects of climate change on land use practices. [1–4].

Carbon sequestration is the practice of removing carbon dioxide (CO2) from the atmosphere and storing it and is one of the many ways to respond to climate change. Carbon sequestration can occur in two basic forms: biological or

DOI: 10.37256/jeee.4220256912

geological. Furthermore, while carbon sequestration is encouraged through various biological and geo-logical processes, it also occurs naturally in the environment on the largest scale. Forests and woodlands are considered one of the best forms of natural carbon sequestration. CO2 is bound to plants during photosynthesis, exchanging it with oxygen as a purified emission, so monitoring forest health and carbon storage capacity is critical to understand the impacts of climate change on this crucial ecosystem service [5–7].

As expected, numerous metrics have been suggested to effectively track vegetation distribution. These metrics need to be statistically robust, demonstrate consistent relationships, respond to the appearance and disappearance of species, remain comparable and consistent across various scales, be cost-effective, and be straightforward to comprehend and implement.

To meet these requirements, many remote sensors have been developed. As a remote sensing technology, LiDAR, which stands for light detection and ranging, has several advantages, including high accuracy, detailed 3D mapping capabilities, long-range measurement capabilities, real-time data collection, and minimal environmental impact. It has found wide applications such as autonomous vehicles, surveying, forestry, mining, agriculture, and environmental monitoring, allowing for accurate terrain analysis and object detection in diverse environments [7,8].

A LiDAR records data in two ways, either discrete return or full waveforms. Discrete return records a single point or a few points, such as the first return, last return, or peak value. The full waveform records the distribution of the returned light energy as it varies with range, which provides better recording of the scattering events and can provide more information than a discrete return system. In vegetation research, full waveform LiDAR can capture the entire canopy profile and vegetation distribution, provide more detailed canopy 3D structure, and is one of the most effective tools for forest remote sensing applications [9–15]. Furthermore, polarized light is ubiquitous in nature and primarily produced by reflection or scattering processes. This is because reflection or scattering often causes changes in the polarization states of the incident light. Therefore, polarized light is a tool that has been applied in many remote sensing applications. All-natural radiation has a certain degree of polarization (although un-polarized radiation can be generated), and differences in the target surface characteristics and morphology will change the laser polarization state. By measuring the polarization states of the received laser beam, the target conditions can be analyzed, which is not available from non-polarimetric LiDAR. Therefore, polarization is important in remote sensing including vegetation and global atmospheric aerosol studies [16–28]. However, current studies mainly use commercial non-polarimetric LiDAR systems for tree species monitoring. Therefore, a LiDAR system with full waveform and polarimetric capability is needed.

Polarimetric LiDAR data analysis involves examining, cleaning, transforming, and modeling data to uncover valuable insights, such as recognizing patterns and relationships within the data, drawing conclusions, supporting decision-making, and ultimately, improving outcomes in the field of study, particularly when processing large and complex datasets that are not amenable to manual analysis. There are multiple aspects and approaches to data analysis, including statistical analysis (as the basis for data analysis), machine learning (ML), deep learning (DL), data mining, neural networks (NNs), artificial intelligence (AI), and more. These methods are not mutually exclusive. In fact, each method intersects and overlaps with others and provides a unique way to extract meaningful information from the data sets [29–33].

The LiDAR vegetation classification is a rapidly growing field that has attracted a lot of attention recently. Vegetation classification using ML is a method in which a model seeks to assign the correct label to a given input. Typically, the dataset is split into training data, validation data, and testing data. The selected model is first trained with the training data, and the model is validated using the validation data to prevent overfitting or to tune the hyperparameters. Then the model is tested using the testing data to evaluate its performance. Once the performance is satisfactory, the model is finalized and can be deployed for real-world data. There are two categories of classification in remote sensing, such as supervised classification (e.g., decision-tree, support vector machine, random forest algorithm), unsupervised classification (e.g., clustering, hierarchical clustering, k-means clustering). The neural networks (e.g., recurrent NNs, convolutional NNs, and Multi-Layer Perceptron) can be either supervised or unsupervised, depending on the way it is trained. Supervised learning requires ground truth data where specific vegetation types are pre-identified and labeled, which is then used to train the ML model to recognize similar patterns in new data. Unsupervised learning, such as clustering, does not require pre-labeled data and can analyze large datasets where detailed ground truth information may be limited or lack precise labels. It can identify groups in the data that may reveal new vegetation patterns or previously unknown plant communities, allowing for preliminary exploration and identification of potential vegetation clusters [34–38]. Hu and Tan [39] used a decision-tree algorithm to differentiate the tree species using the intensity signals of the tree species captured by the customized multiwavelength

airborne polarimetric LiDAR system (MAPL) data, and found the re-substitutional accuracy and k-fold validation accuracy are 96.8% and 95.0%, respectively, even though the process is complex with long classification steps. Then the full width at half maxima (FWHMs) of the LiDAR waveform were added as another feature for supervised decision-tree classification, the corresponding accuracy were improved to 98.9% and 94.4% respectively, and the classification process steps reduced to about one third of the previous process. In addition, using unsupervised classification methods, such as clustering methods (e.g., k-means, k-medoids, Gaussian mixture model), clustering accuracies have reached around 80% [40].

Recent progress in sensor technologies has facilitated the acquisition of high-resolution remote sensing data. These data can reveal vegetation canopies with more fine details. To leverage the growing stream of new sensor data to meet the rising needs on vegetation assessment and monitoring, efficient, accurate, and flexible data analysis is needed. In this regard, DL algorithms such as deep convolutional neural networks are currently opening new avenues to achieve high prediction accuracy and independently uncovering the data features. A series of studies have shown that convolutional neural network (CNN) method can represent spatial patterns effectively, thereby enabling the extraction of various vegetation characteristics from remote sensing data [41–49]. The overall accuracy of the classification can reach above 80%, even between 94 and 97% [44,45]. Zorzi et al. used CNNs to classify full-waveform airborne LiDAR data to distinguish between six categories: ground vegetation, buildings, power lines, transmission towers, and street paths, with an overall accuracy of 92.6% [46]. Leigh and Magruder [49] used dual-wavelength, near-infrared (NIR) and green (GN), and full-waveform airborne LiDAR data for surface classification and vegetation characterization and found that the combination of NIR and GN response could improve the overall classification accuracy by up to 6%.

This work, as an extension of previous studies, uses a CNN approach, where the numerical values of the peak reflectance intensities and FWHMs extracted from the multiwavelength polarimetric LiDAR were used as inputs. We want to explore and evaluate the performance of CNN in polarimetric lidar data classification. CNN classification was performed under four different scenarios: SCENARIO 1, dual-wavelength and dual-polarization; SCENARIO 2, one wavelength at 1064-nm with dual-polarization; SCENARIO 3, one wavelength at 532-nm with dual-polarization; and SCENARIO 4, dual-wavelength with co-polarization only. To achieve the objectives, several efforts are required, beginning with data collection and preparation, progressing to CNN, and concluding with an analysis of how various factors affect the results and potential areas for future enhancements.

2. Multiwavelength Airborne Polarimetric LiDAR System

The sensor used in this study is the multiwavelength airborne polarimetric LiDAR system (MAPL) designed specifically for vegetation remote sensing. The MAPL has three main parts, the laser source, the receiver subsystem, and the data acquisition subsystem, as shown in Figure 1. The system works by controlling a digital delay-pulse generator through an RS-232 interface by a computer to exchange serial binary data between the two devices. A transistor-transistor logic (TTL) signal is then generated by the delay generator to control the precise timing of the LiDAR. The laser emits two laser pulses at 1064-nm (NIR) and 532-nm (GN) simultaneously. The laser pulses are backscattered by the vegetation and received by the four photomultiplier-tube (PMT) detectors. They enable the detection of both co-polarized and cross-polarized laser beams. The outputs of the PMT detectors are digitized and then sent to the computer. The data is stored in the computer and post-processed. More detailed parameters of the MAPL can be found in [50–52].

A generic LiDAR equation for the received laser power is described by [51]

$$P_R = \frac{\pi P_T \rho_T D^2}{16R^2} \cdot {T_A}^2 \cdot \eta_T \cdot \eta_R, \tag{1}$$

where P_R is the received power of the MAPL, P_T is the transmitted power of the MAPL, R is the range from the MAPL to the target, D is the diameter of the optical detector, ρ_T is the target reflectivity, T_A is the one-way atmospheric transmission coefficient from the MAPL to the target, η_T is the transmitter transmission efficiency, and η_R is the receiver transmission efficiency. It can be seen that for extended targets, the received power is inversely proportional to the square of the distance.

The received power has two polarization directions, namely co-polarization P_{RCO} and cross-polarization P_{RX}. The cross-polarization ratio is defined as

$$\delta = \frac{P_{RX}}{P_{RCO}}, \quad (2)$$

It is used to characterize the laser scattering properties of a target in many LiDAR applications [52].

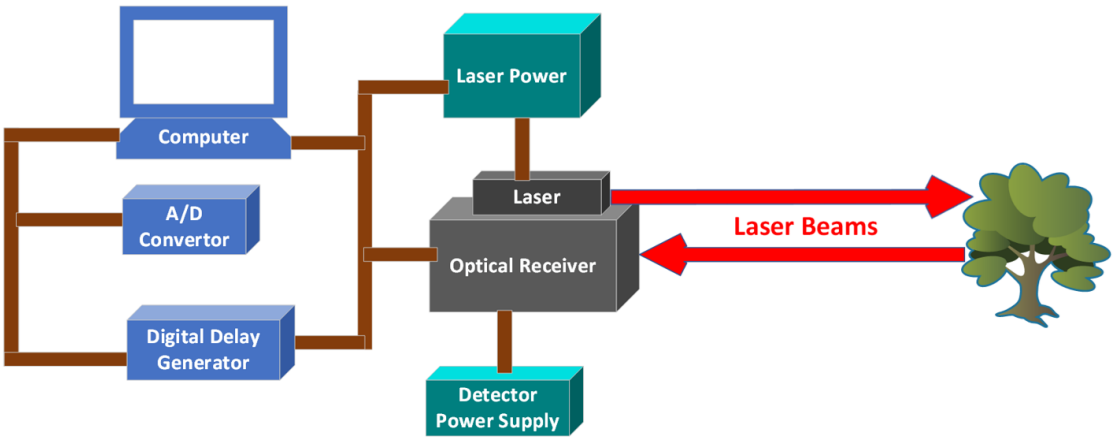

Figure 1. Schematic diagram of the multi-wavelength airborne polarimetric LiDAR system (MAPL).

3. Data Collection and Preparation

This study aims to classify the tree species using CNN based on the combinations of the peak and FWHM values. We also want to evaluate the performance in terms of effectiveness and accuracy of different scenarios for polarized and simulated unpolarized LiDAR, and dual-wavelength and single wavelength LiDAR, in order to identify the uniqueness and contribution of each numerical feature extracted from the waveform data to the overall classification accuracy.

3.1 *Data Collection*

Data collections were performed on the ground as illustrated in Figure 1. Five tree species were selected for this study. They are coniferous trees (blue spruce, ponderosa pine, and Austrian pine) and deciduous trees (ash and maple) with different biophysical features. Different biophysical characteristics of trees are crucial for identifying tree species because they represent unique adaptations, evolutionary history, and interactions with the environment. These characteristics—including leaf shape, bark texture, branch morphology, and growth habit—are represented in LiDAR signals, such as reflectance and polarization. These signals are key to distinguishing tree species and understanding their ecological roles. These tree species used in this study are common in eastern South Dakota. During data collection, the individual tree was detected by the MAPL through four different channels. At each study site, at least hundreds of measurements were taken using the LiDAR. During each MAPL operation, wind speed at each study site was sampled. All field measurements were performed under clear weather during midday to ensure data consistency and minimize the effects of changing sun brightness. Since the green laser beam is visible, it is easy to aim at the tree canopy. At the test sites, the distances between the trees and the MAPL were kept at approximately 500 meters. Variations in returns due to range differences were normalized by multiplying the square of the range data. Furthermore, to reduce data variation and improve consistency during data collection, the LiDAR was carefully calibrated before taking any measurements.

3.2 *MAPL Data Preparation*

The LiDAR data collection was done using a self-developed LabVIEW program. It was also used to display the real-time LiDAR data on the computer screen. Four different channels were used to retrieve information about the two orthogonal and linear polarization states of the signals at two wavelengths. This means that after any single LiDAR shot over the tree canopy, these four channels collect information simultaneously. All these recorded signals were calibrated similar to the work of [51]. The output data are read into MATLAB for further processing or analysis.

Figure 2 shows the typical single shot MAPL pulse returning waveforms from a ponderosa pine and a maple. In this study, the peak reflectance intensities and their corresponding FWHMs were used as the features for later classification.

Data preprocessing includes radiometric calibration, range calibration, and outlier removal. Radiometric calibration is achieved using a canvas calibration standard [51]. Range calibration is achieved by normalizing all LiDAR data by range (as in Eq. (1)), i.e., multiplying the LiDAR return data by the square of the distance [52]. Finally, a criterion of three standard-deviations from the mean was used to determine if a data point is an outlier and needs to be removed [39].

After cleaning up the outliers, the captured datasets of the polarized waveform signals contain a total of 16,848 valid signal feature datasets, including a total of 8,424 peak reflectance intensity values and 8,424 corresponding FWHM values, which can be extracted using a customized program written in MATLAB. To simulate the data from a nonpolarimetric LiDAR, the co-polarization and cross-polarization at each wavelength were summed up, respectively. This resulted in half the datasets, i.e., a total of 8,424 datasets of non-polarized LiDAR, containing 4,212 peak reflectance intensity values and 4,212 corresponding FWHMs. The resulting tree data used in this study are listed in Table 1.

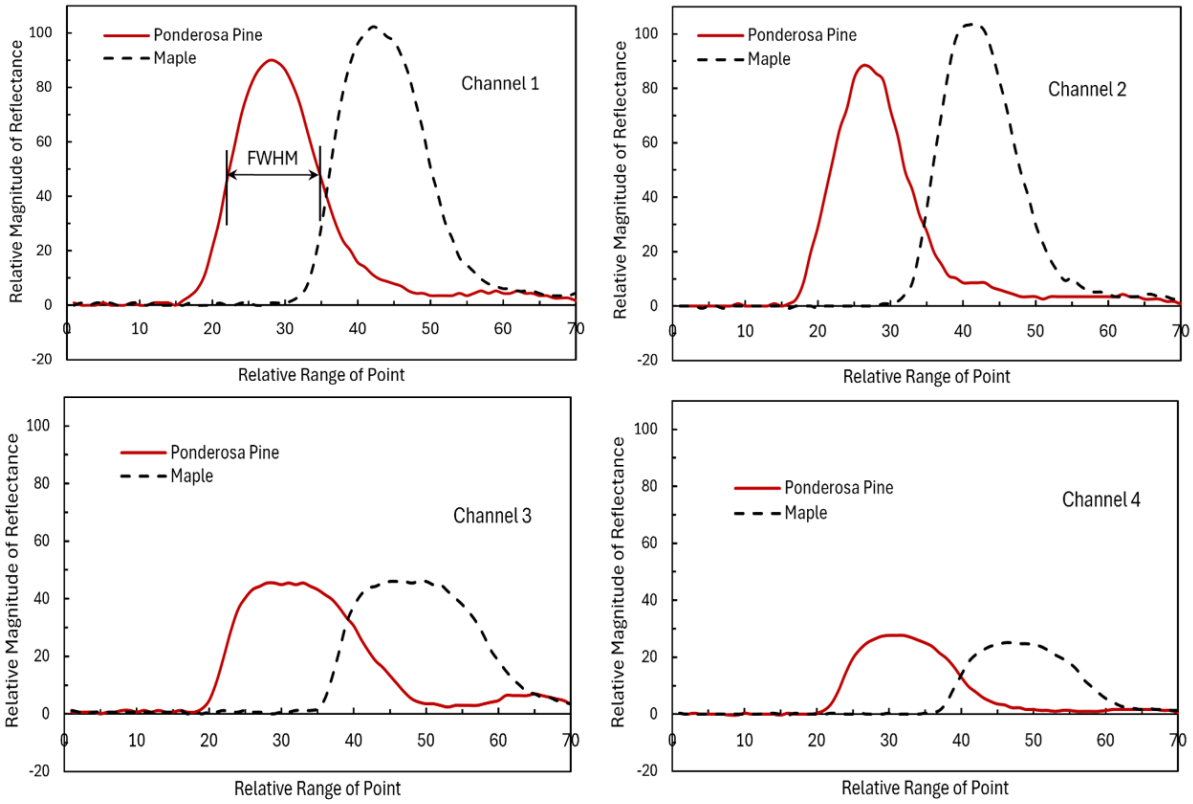

Figure 2. Typical MAPL waveforms from ponderosa pine and maple. (Ch1: NIR co-polarized, Ch2: NIR cross-polarized, Ch3: GN co-polarized, and Ch4: GN cross-polarized waveforms, respectively.)

Table 1. Number of Counts and distribution of tree datasets used in this study.

Species (Classifier)	Species Count	Polarized Datasets	Non-polarized Datasets	Percent
Blue Spruce	244	1,952	976	11.59%
Ash	277	2,216	1,108	13.15%
Ponderosa Pine	795	6,360	3,180	37.75%
Austrian Pine	318	2,544	1,272	15.10%
Maple	472	3,776	1,888	22.41%
Total	2,106	16,848	8,424	100.00%

4. CNN for Tree Classification

Deep Learning (DL) is a subset of machine learning (ML) technology that uses multilayer artificial neural networks (ANNs), called deep neural networks (DNNs), to simulate the complex decision-making capabilities of the human brain and has allowed many applications to achieve high accuracy. DNNs are able to model and capture complex connections between input and output. A CNN approach is adopted in this research. It is a regularized feed-forward neural network characterized by convolutional layers that optimize self-learned features through filters (or kernels) and generate activation maps. These activation maps are then processed by pooling layers, which aggregate the low-resolution data to reduce the dimensionality of the representation and make processing computationally more efficient. The convolutional and pooling layers are repeated several times, gradually transforming the images into a low-resolution activation map. This type of network has been used to process and predict many different types of data, including text, digits, images, and audio [33,53–55]. In this study, a general architecture of the CNN model was adopted and numerical data (such as the peak intensity values and FWHMs) were used as the event features for CNN classification, and the schematic diagram of the model is shown in Figure 3. In the general architecture of the CNN model, several primary components that need to be noted are as follows:

- Convolutional Layers are the core components of a CNN model, where a small filter (kernel) is applied to the raw data or image, extracting features such as edges or textures by sliding across the image or reading the numerical data at different positions. By stacking multiple convolutional layers, CNNs can progressively learn more complex features from the input data (images or numerical digits), moving from basic patterns to higher-level object parts.
- Rectified linear units (ReLUs) serve as crucial activation functions within NNs. They are often used multiple times in a single network, usually after convolutional layer. A ReLU layer consists of neurons that implement the function

$$f(x) = \max(0, x). \tag{3}$$

- Incorporating these layers enhances the non-linearity of the network while keeping the receptive fields of the convolutional levels unchanged.
- Pooling layers are commonly applied following convolutional layers to decrease the spatial dimensions of the feature map, typically through operations such as maximizing pooling, which selects the maximum value in a local region, helping to maintain important features while reducing computational complexity.
- Fully Connected Layers: After the feature extraction, the output of the convolutional and pooling layers is flattened into a vector and fed into fully connected layers like a traditional NN, to perform the final classification or prediction. In a CNN model, a "fully connected layer" is essentially a type of "hidden layer" where every neuron in the layer is connected to every neuron in the previous layer, which means that a fully connected layer is considered a specific type of hidden layer within a CNN architecture; while not all hidden layers are necessarily fully connected, a fully connected layer is always considered a hidden layer. To put it more clearly, a hidden layer is any layer within a NN that is not the input or output layer, and it can consist of different types of connections, including fully connected ones, which enables the network to learn global patterns across the entire images or numerical digits.
- SoftMax Activation Function is simply a function as

$$Y = \text{softmax}(X). \tag{4}$$

  where X represents the input data, and the output Y will be the normalized probability distribution after applying softmax across the channel dimension of the input data. In terms of the training phase, CNNs can suffer from the age-old problem of overfitting. To mitigate this, regularization techniques are usually employed to intervene in the optimization process during the training phase.
- Data Augmentation creates additional training data by applying random transformations (e.g., rotations, scaling) to existing data to expose the model to a greater variety of examples.

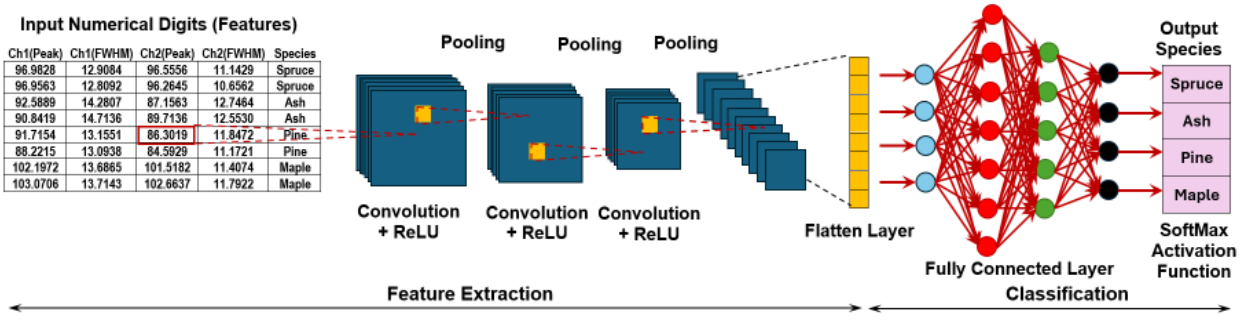

Figure 3. Schematic diagram of CNN architecture for tree classification.

Several factors can pose considerable challenges to the practical computation of CNNs, including dimensionality, the number of layers (and units per layer), learning rates, initial weights, and the optimization of these parameters—a process that can become intractable in terms of time and computational resources.

5. Experimental Results and Discussion

In this study, four scenarios were selected for modeling and analysis: (1) using data from NIR co-polarized and cross-polarized waveforms, and GN co-polarized and cross-polarized waveforms; (2) using two NIR polarized channels only (i.e., NIR co-polarized and NIR cross-polarized waveforms); (3) using two GN polarized channels (i.e., GN co-polarized and GN cross-polarized waveforms); and (4) using two non-polarized waveforms (i.e., NIR and GN non-polarized waveforms as listed in Table 1. Finally, the prediction accuracies of different hidden layer CNN models under these four scenarios were compared and analyzed.

The numerical data in this study refers to the training features. The numerical data was used to train the CNN models. After training, the CNN models will be able to predict tree classes. For SCENARIO 1, there are 8 features, i.e., the peak and the FWHM for each channel. The dataset format as the input datasets for SCENARIO 1 is shown in Table 2. The names of the last column are the tree classes to be predicted after training.

Table 2. Dataset format for SCENARIO 1.

Ch1Peak	Ch1FWHM	Ch2Peak	Ch2FWHM	Ch3Peak	Ch3FWHM	Ch4Peak	Ch4FWHM	Class
96.556	12.908	96.083	11.143	44.308	20.231	25.997	17.292	B. Spruce
102.54	12.879	96.083	10.375	43.535	20.248	25.672	17.219	B. Spruce
100.83	13.066	95.209	10.861	43.157	20.500	25.867	17.319	B. Spruce
97.410	12.932	94.336	10.944	43.733	20.316	25.775	17.117	B. Spruce
:	:	:	:	:	:	:	:	:
106.81	13.996	103.07	12.104	46.610	20.990	25.022	17.711	Maple
109.37	13.934	102.20	11.562	46.034	20.901	25.053	18.000	Maple
105.95	13.902	101.32	11.487	46.610	21.495	25.115	17.670	Maple
108.52	13.814	102.20	11.761	46.353	21.972	25.033	18.105	Maple
Up to 2106 rows for digital features								

There are five tree categories/classes: blue spruce, ash, ponderosa pine, Austrian pine, and maple, with a total of 2106 data instances. For each scenario, 70%, 15%, and 15% of the data were taken for training, validation and testing, respectively. For example, SCENARIO 1 has 1474, 315, and 317 data instances. Considering the consistency and fairness of the CNN model training, validation, and testing, the data instance was randomly selected from the entire dataset for training, validation, and testing.

The next CNN modeling design is the layout of the layer array of the CNN model, and Table 3 lists a typical CNN model layout designed in this study. It is worth noting that Layer Order 2 can have various fully connected layers to be able to evaluate the effect of the number of connected layers (as a variation of hidden layers in the feature extraction process) on the final classification accuracy. In Layer Order 5, the classification process has five fully connected layers (five fixed number of hidden layers), which aimed to effectively express the classification probability (classification accuracy) based on the processed feature expression information.

Table 3. Layout of the CNN model layer array.

Order No.	Layer Name	Notes
1	Feature Input	4-8 features (corresponding to the different scenarios) with 'zscore' normalization (a Gaussian distribution)
2	Fully Connected	Up to dozens of fully connected layers as variable hidden layers
3	Batch Normalization	Normalizes the activations of a layer within a mini batch
4	ReLU	Rectified linear unit, a non-linear activation function
5	Fully Connected	Five fully connected layers
6	SoftMax	A function takes a vector of real numbers as input and transforms it into a probability distribution over multiple class
7	Classification Output	For Computing the cross-entropy loss for classification tasks

It is worth noting that there are two "fully connected' layers in the constructed model. This paper defines the number of the first fully connected layers (i.e., the number of the hidden layers) up to dozens of fully connected layers as a variable and studied its effect on the prediction accuracy. The number of the second fully connected layers remains unchanged, and usually five layers are used to reach satisfactory performance.

After completing the CNN model design, the next step is to define the options for running the model. The options defined for the four scenarios used the same settings, and the main training process parameters are: MaxEpochs=30, MiniBatchSize=6, Shuffle=every-epoch, and Plots= training-progress. Figure 4 shows the changes in Training Loss, Training Accuracy, Validation Loss, and Validation Accuracy for scenarios 1, 2, 3, and 4 during a typical CNN training or validation process with 5 hidden layers. Since the training data and validation data were randomly shuffled and selected from the dataset each time, each training or validation process is slightly different. Also, since Training Loss and Training Accuracy during the training process are volatile, the data of the Training Loss and Training Accuracy shown in Figures. 4a and 4b were fitted to an exponential decay function (Training Loss) and a logistic growth function (Training Accuracy), respectively. As can be seen from Figure 4 that SCENARIO 1 exhibits lower training and validation losses (error measurements), as well as higher training and validation accuracy. On the other hand, SCENARIO 3 exhibits higher training and validation losses and lower training and validation accuracy in comparison. Figure 5 shows the confusion matrices of the prediction accuracy after training and validation processes for SCENARIO 3, with the number of hidden layers being 1 (Figure 5a) and 5 (Figureure5b). As the number of the hidden layers increases from 1 to 5, the number of correct predictions increases, while that of the incorrect predictions decreases.

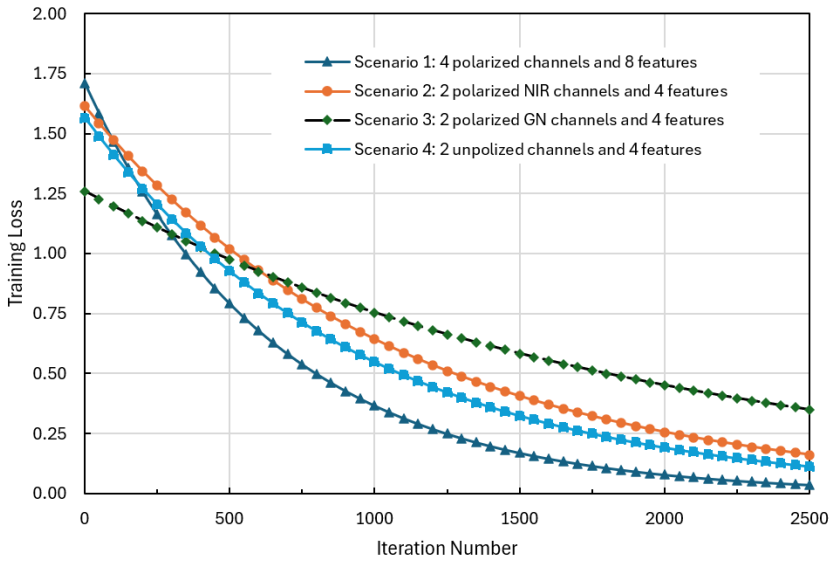

(a)

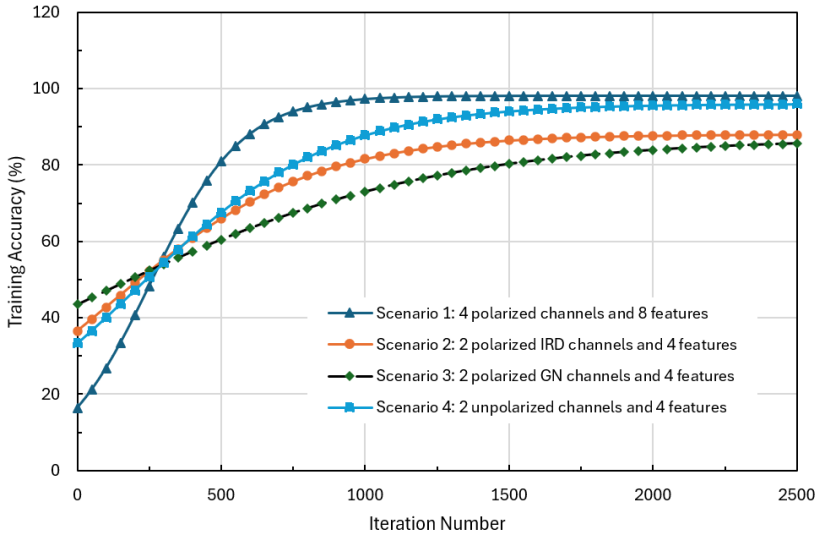

(b)

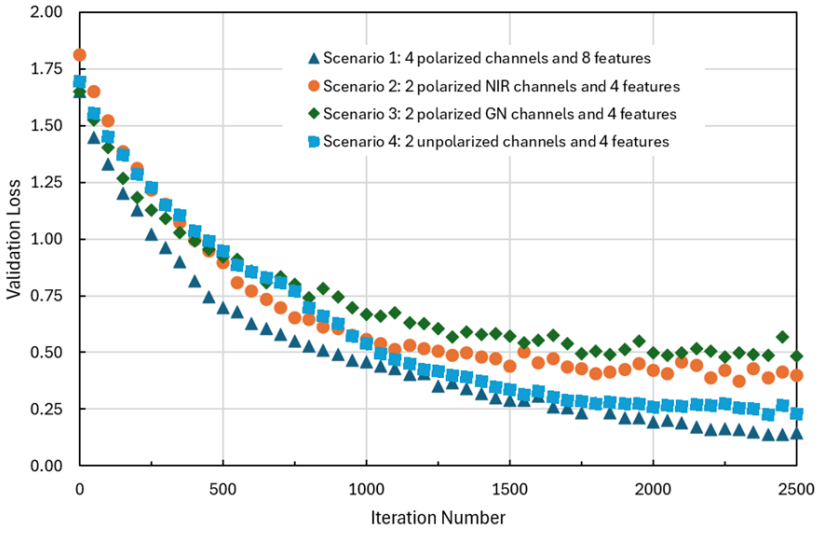

(c)

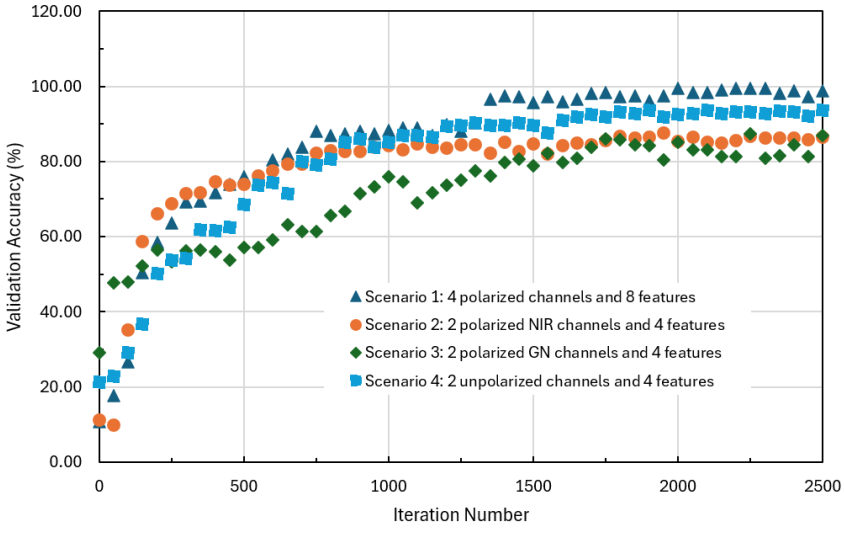

(d)

Figure 4. Training Loss (a), Training Accuracy (b), Validation Loss (c) and Validation Accuracy (d) vs. iteration number during a typical run of the training or validation progress for SCENARIO 1, 2, 3 and 4 with 5 hidden layers in the feature extraction.

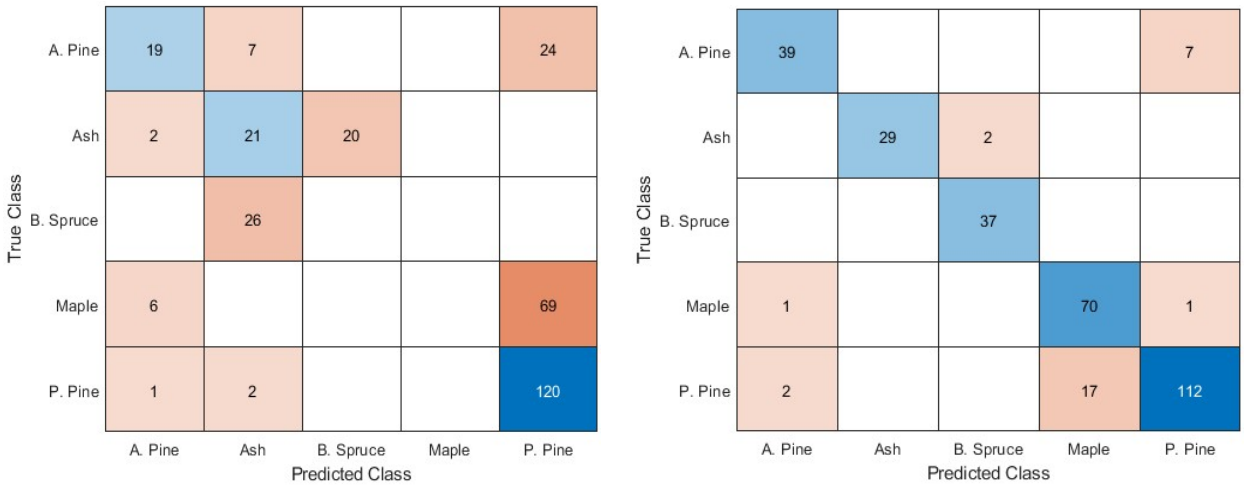

Figure 5. Confusion matrices of prediction (test) accuracy after training and validation processes for SCENARIO 3. (a) with 1 hidden la yer and (b) with 5 hidden layers.

Finally, Figure 6 shows the comparative analysis of the predication accuracy vs. the number of hidden layers for the four scenarios. Here the prediction accuracy is calculated as follows:

$$\text{Prediction Accuracy} = \frac{\text{Number of corectted predicted tree species}}{\text{Number of all tree species}} \times 100\% \quad (5)$$

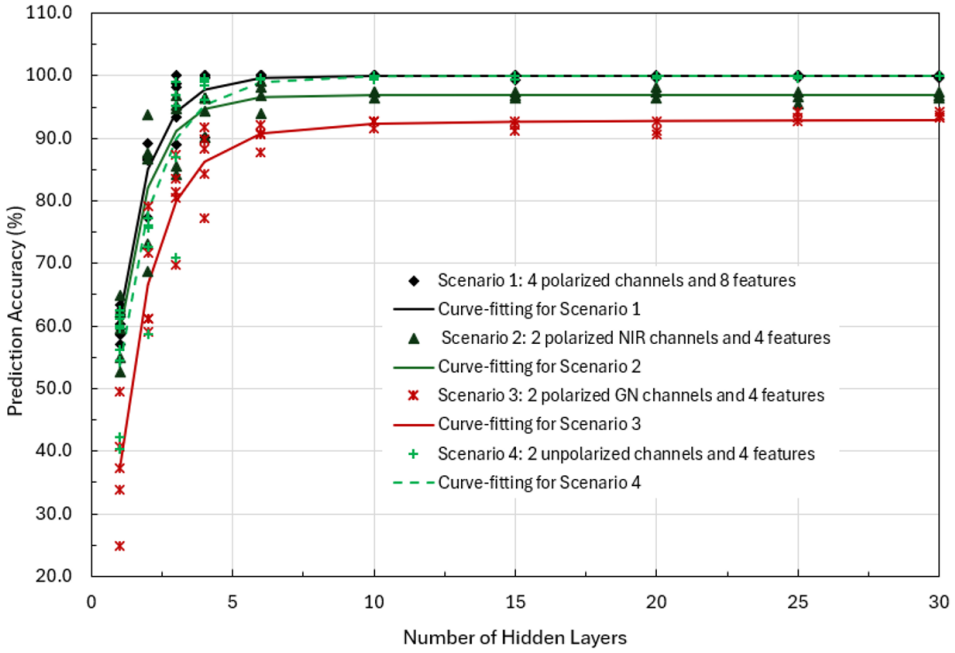

Figure 6. Predication accuracy vs. number of hidden layers for all four scenarios.

For easy comparison, the prediction accuracy data for each scenario was curve-fitted. As can be seen from Figure 6, in SCENARIO 1 (4 polarized channels and 8 features, as shown by the black "♦" symbol and curve-fitted by the black solid line), as the number of the hidden layers increases from 1 to 5, the prediction accuracy increases rapidly from about 61% to about 99%, and then gradually approaches (converges to) 100%. The small fluctuations i ndicate that the data is randomly selected during each run, each modeling should be different, and the prediction accuracy of each modeling is relatively close (small deviation). In SCENARIO 2 (2 polarized NIR channels and 4 features, as shown by the green "▲" symbol and curve-fitted by the dark blue solid line), since only NIR polarized LiDAR data

was considered, as the number of the hidden layers increases from 1 to 5, the prediction accuracy increases rapidly from about 59% to about 96%, and after large fluctuations, it steadily approaches (converges to) about 97% (it did not reach 100% in the end). Similarly, in SCENARIO 3 (2 polarized GN channels and 4 features, as shown by the "×" symbol and curve-fitted by the dark red solid line), as the number of the hidden layers increases from 1 to 5, the prediction accuracy increases rapidly from about 37% to about 89%, fluctuates greatly, and then steadily approaches (converges to) 93% (it did not reach 100% in the end). Finally, in SCENARIO 4 (2 unpolarized NIR and GN channels and 4 features, as shown by the "+" symbols and curve-fitted by the green dashed line), as the number of the hidden layers increases from 1 to 5, the prediction accuracy increases rapidly from about 54% to about 97%, fluctuates greatly, and then approaches (converges to) 100%.

On the other hand, when the hidden layers in a CNN model become too large (with a high number of neurons), the main drawback is overfitting (when the number of hidden layers becomes very large compared to the complexity of the problem), where the network learns the training data too closely, resulting in poor performance on new, unseen data, while increasing training time and computational complexity. Therefore, the numerical feature data from SCENARIO 1 with dual-wavelengths (NIR and GN) and peak intensities and FWHMs are the most suitable data format for CNN tree classification prediction, with high stability, high prediction accuracy, and less hidden layers.

There are several limitations in this research. First, as a proof-of-concept study, the data were collected on the ground. Future airborne data will need to be collected and processed to demonstrate the effectiveness of the technique. Second, only five tree species were studied in this paper. The inclusion of more tree species would make the research more vigorous. In addition, future research should address radiometric calibration using more reliable calibration standards instead of commercial canvas tarps. In addition, better power regulators can provide power with less noise. It is also important to collect more tree data and study other features to deepen our understanding of the classification process. Furthermore, a theoretical framework for laser polarimetric scattering in tree canopies has yet to be established. Developing this theory would significantly enhance the understanding of LiDAR waveform and aid in creating more efficient classification methods. On the other hand, it is necessary to consider exploring other ML methods to add or adopt more effective features in the algorithms of the deep learning methods, such as adopting the entire reflectance signal profile/image to improve the feasibility and accuracy of tree species classification.

6. Conclusions

The LiDAR data from the MAPL offer advantages for vegetation and forest remote sensing. Featuring dual-wavelength, dual-polarization, and full-waveform capabilities, it is currently the only system of its kind for vegetation research. In this study, tree species classification was successfully performed using CNN models, and the following main conclusions were drawn:

- The CNN approach is an effective and accurate method for tree classification.
- Polarimetric numerical features (peak intensities and FWHMs) have been proven to be effective features for tree classification. Polarimetric diversity enhances measurement and provides more information about the target characteristics.
- The prediction accuracy the CNN model has a logistic growth function relationship with the number of hidden layers designed during the feature extraction process. For our dataset, using 5 hidden layers provides a good balance between performance and computational cost. The training loss and the validation loss have exponential decay function relationships with the process iteration number. The training accuracy and validation accuracy have logistic growth function relationships with the process iteration number.
- SCENARIO 1 has the highest stability (least deviation) and approaches maximum accuracy the fastest when the number of hidden layers is greater than or equals to 5.
- This method can distinguish between Austria pine and Ponderosa pine, which have only subtle differences.
- The method developed in this study can be extended to new data and even other vegetation classification applications.

Conflict of Interest

The authors declare that there are no financial interests, commercial affiliations, or other potential conflicts of interest that could have influenced the objectivity of this research or the writing of this paper.

Data Availability

Data are available from the authors upon reasonable request.

Acknowledgments

The authors would like to thank former graduate students Ali Haider and Nabeen Thakur for assisting in field data collections.

References

[1] United States Environmental Protection Agency (EPA). Climate Change Impacts on Agriculture and Food Supply. September 23rd, 2024, access on October 16, 2024, at Climate Change Impacts on Agriculture and Food Supply | US EPA.

[2] Lipton, D.; Rubenstein, M. A.; Weiskopf, S. R. Ch. 7: Ecosystems, ecosystem services, and biodiversity. In: Impacts, risks, and adaptation in the United States: Fourth national climate assessment, volume II. U.S. Global Change Research Program, Washington, DC, 2018, p. 270.

[3] Lipton, D.; Rubenstein, M. A.; Weiskopf, S. R. Ch. 7: Ecosystems, ecosystem services, and biodiversity. In: Impacts, risks, and adaptation in the United States: Fourth national climate assessment, volume II. U.S. Global Change Research Program, Washington, DC, 2018, p. 276.

[4] McElwee, P. D., et al. Ch. 8: Ecosystems, ecosystem services, and biodiversity. Fifth National Climate Assessment. U.S. Global Change Research Program, Washington, DC, 2023, p. 8-18.

[5] Vose, J.M., et al. Ch. 6: Forests. In: Impacts, risks, and adaptation in the United States: Fourth national climate assessment, volume II. U.S. Global Change Research Program, Washington, DC, 2018,p. 234.

[6] Canto-Sansores, W. G.; López-Martínez, J. O.; González, E. J.; Meave, J. A.; Hernández-Stefanoni, J. L.; Macario-Mendoza, P. A. The importance of spatial scale and vegetation complexity in woody species diversity and its relationship with remotely sensed variables. ISPRS Journal of Photogrammetry and Remote Sensing 2024, 216, 142-253.

[7] Frachetti, M. D.; Berner, J.; Liu, X.; Henry, E. R.; Maksudov, F.; Ju, T. Large-scale medieval urbanism traced by UAV-lidar in highland Central Asia. Nature 2024, 21 pages. https://doi.org/10.1038/s41586-024-08086-5.

[8] Rapinel, S.; Hubert-Moy, L. One-class classification of natural vegetation using remote sensing: a review. Remote Sensing 2021, 13(10), 1892.

[9] Salas, E. A. Waveform LiDAR concepts and applications for potential vegetation phenology monitoring and modeling: a comprehensive review. Geo-spatial Information Science 2021, 24(2), 179-200.

[10] Dubayah, R. O.; Drake, J. B. Lidar Remote Sensing for Forestry, Journal of Forestry, Volume 98, Issue 6, June 2000, Pages 44–46, https://doi.org/10.1093/jof/98.6.44.

[11] Cao, L.; Coops, N. C.; Hermosilla, T.; Innes, J.; Dai, J.; She, G. Using small-footprint discrete and full-waveform airborne LiDAR metrics to estimate total biomass and biomass components in subtropical forests. Remote Sensing 2014, 6(8), 7110-7135.

[12] Dong, P.; Chen, Q. LiDAR Remote Sensing and Applications (1st ed.). CRC Press. 2017. https://doi.org/10.4324/9781351233354.

[13] Frachetti, M. D.; Berner, J.; Liu, X.; Henry, E. R.; Maksudov, F.; Ju, T. Large-scale medieval urbanism traced by UAV-lidar in highland Central Asia. Nature, 634, 1118-1124, 2024, https://doi.org/10.1038/s41586-024-08086-5.

[14] Lefsky, M. A.; Cohen, W. B.; Parker, G. G.; Harding, D. J. Lidar Remote Sensing for Ecosystem Studies: Lidar, an emerging remote sensing technology that directly measures the three-dimensional distribution of plant canop

ies, can accurately estimate vegetation structural attributes and should be of particular interest to forest, landscape, and global ecologists, BioScience 2002, 52(1), 19–30, https://doi.org/10.1641/0006-3568(2002)052[0019:LRSFES]2.0.CO;2
[15] Lim, K.; Treitz, P.; Wulder, M.; St-Onge, B.; Flood, M. LiDAR remote sensing of forest structure. Progress in Physical Geography: Earth and Environment 2003, 27(1), 88-106. https://doi.org/10.1191/0309133303pp360ra.
[16] Kalshoven, J.E.; Tierney, M.R.; Daughtry, C.S.T.; McMurtrey, J.E. Remote sensing of crop parameters with a polarized, frequency-doubled Nd:YAG laser, Applied Optics 1995, 34, 2745-2749.
[17] Liu, X.; Zhang, X.; Zhai, X.; Li, L.; Zhou, Q.; Chen, X.; Li, X. Polarization lidar: principles and applications. Photonics 2023, 10(10), 1118.
[18] Kong, Z.; Ma, T.; Zheng, K.; Cheng, Y.; Gong, Z.; Hua, D.; Mei, L. Development of an all-day portable polarization Lidar system based on the division-of-focal-plane scheme for atmospheric polarization measurements. Opt. Express 2021, 29, 38512–38526.
[19] Potsdam, K. H.; Itzerott, S.; Weltzien, C.; Spengler, D. Agricultural monitoring using polarimetric decomposition parameters of Sentinel-1 data. Remote Sensing 2021, 13(4), 575.
[20] Haldar, D.; Dave, R.; Dave, V. A. Evaluation of full-polarimetric parameters for vegetation monitoring in rabi (winter) season. The Egyptian Journal of Remote Sensing and Space Science. 2018, 21, S67-S73.
[21] Liu, Y.; Wang, L.; Zhu, S.; Zhou, X.; Liu, J.; Xie, B. Agricultural application prospect of fully polarimetric and quantification S-band SAR subsystem in Chinese high-resolution aerial remote sensing system. Sensors 2024, 24(1), 236.
[22] Jin, H.; Mountrakis, G. Fusion of optical, radar and waveform LiDAR observations for land cover classification. ISPRS Journal of Photogrammetry and Remote Sensing 2022, 187, 171-190.
[23] Hancock, S.; Armston, J.; Li, Z.; Gaulton, R.; Lewis, P.; Disney, M.; Danson, F. M.; Strahler, A.; Schaaf, C.; Anderson, K.; Gaston, K. J. Waveform lidar over vegetation: an evaluation of inversion methods for estimating return energy. Remote Sensing of Environment 2015, 164, 208-224.
[24] Fieber, K. D.; Davenport, I. J.; Ferryman, J. M.; Gurney, R. J.; Walker, J. P.; Hacker, J. M. Analysis of full-waveform LiDAR data for classification of an orange scene. ISPRS Journal of Photogrammetry and Remote Sensing 2013, 82, 63-68.
[25] Tan, S.; Narayanan, R. M.; Shetty, S. K. Polarized lidar reflectance measurements of vegetation at near-infrared and green wavelengths. International Journal of Infrared and Millimeter Waves 2005, 26, 1175-1194.
[26] Tan, S.; Haider, A. A comparative study of polarimetric and non-polarimetric lidar in deciduous—coniferous tree classification. 2010 IEEE International Geoscience and Remote Sensing Symposium, pp. 1178-1181.
[27] Tan, S.; Narayanan, R.; Helder, D. Polarimetric reflectance and depolarization ratio from several tree species using a multiwavelength polarimetric lidar. Proc. SPIE, Polarization Science and Remote Sensing II, Vol. 5888-5923, 2005.
[28] Tan, S.; Johnson, S.; Z. Gu, Z. Laser depolarization ratio measurement of corn leaves from the biochar and non-biochar applied plots. Optics Express 2018, 26(11), 14295-14306.
[29] Brown, M. S. Transforming Unstructured Data into Useful Information, in book: Big Data, Mining, and Analytics, 1st Edition, Auerbach Publications, 2014, 211–230, doi:10.1201/b16666-14, ISBN 978-0-429-09529-0.
[30] Hu, Z.; Zhou R. Review on some important research progresses in biodegradable plastics/polymers. Recent Progress in Materials 2024, 6(2), 015.
[31] Shang, C.; You, F. Data analytics and machine learning for smart process manufacturing: recent advances and perspectives in the big data era. Engineering 2019, 5(6), 1010-1016.
[32] Piaser, E.; Villa, P. Evaluating capabilities of machine learning algorithms for aquatic vegetation classification in temperate wetlands using multi-temporal Sentinel-2 data. International Journal of Applied Earth Observation and Geoinformation 2023, 117, 103202.
[33] Ciaburro, G. MATLAB for Machine Learning – Unlock the Power of Deep Leaning for Swift and Enhanced Results. 2nd Edition, Packt Publishing, Birmingham UK, 2024.
[34] Matyukira, C.; Mhangara, P. A advances in vegetation mapping through remote sensing and machine learning techniques: a scientometric review. European Journal of Remote Sensing 2024, 57(1), 2422330.
[35] Barhate, D.; Pathak, S.; Singh, B. K.; Jain, A.; Dubey, A. K. A systematic review of machine learning approaches in plant species detection. Smart Agricultural Technology 2024, 9, 100605.
[36] Goel, L.; Nagpal, J. A systematic review of recent machine learning techniques for plant disease identification and classification. IETE Technical Review 2023, 40(3), 423-439.

[37] Yang, M.-S.; Lai, C.-Y.; Lin, C.-Y. A robust EM clustering algorithm for Gaussian mixture models. Pattern Recognition 2012, 45, 3950-3961.
[38] Zhang, Y.; Li, M.; Wang, S.; Dai, S.; Zhu, E.; Xu, H.; Zhu, X.; Yao, C.; Zhou, H. Gaussian mixture model clustering with incomplete data. ACM Trans. Multimedia Comput. Commun. Appl. 2021, 17(1s), 6.
[39] Hu, Z.; Tan, S. Assessment of tree species classification by decision tree algorithm using multiwavelength airborne polarimetric LiDAR data. Electronics 2024, 13(22), 4534.
[40] Hu, Z.; Tan, S. Supervised and unsupervised machine learning approaches for tree classification using multi-wa velength airborne polarimetric LiDAR, Smart Agriculture Technology, 2025, 11-100872, https://doi.org/10.101 6/j.atech.2025.100872.
[41] Kattenborn, T.; Eichel, J.; Fassnacht, F. E. Convolutional neural networks enable efficient, accurate and fine-grained segmentation of plant species and communities from high-resolution UAV imagery. Sicentific Reports 2019, 9, 17656.
[42] Kattenborn, T.; Leitloff, J.; Schiefer, F.; Hinz, S. Review on convolutional neural networks (CNN) in vegetation remote sensing. ISPRS Journal of Photogrammetry and Remote Sensing 2021, 173, 24-49.
[43] Jasim, B. S.; Jasim, O. Z.; AL-Hameedawi, A. N. A review for vegetation vulnerability using artificial intelligent (AI) techniques. AIP Conference Proceedings 2024, 3092(1), 040002.
[44] Boston, T.; Dijk, A. V.; Thackway, R. U-net convolutional neural network for mapping natural vegetation and forest types from landsat imagery in Southeastern Australia. Journal of Imaging 2024, 10, 143.
[45] Yu, H.; Jiang, D.; Peng, X.; Zhang, Y. A vegetation classification method based on improved dual-way branch feature fusion U-net. Frontiers in Plant science 2022, 13, 1047091.
[46] Zorzi, S.; Maset, E.; Fusiello, A.; Crosilla, F. Full-waveform airborne LiDAR data classification using convolutional neural networks. IEEE Transactions on Geoscience and Remote Sensing 2019, 57(10), 8255-8261.
[47] Ahmed, K. R.; Akter, S.; Marandi, A.; Schüth, C. A simple and robust wetland classification approach by using optical indices, unsupervised and supervised machine learning algorithms. Remote Sensing Applications: Society and Environment 2021, 23, 1000569.
[48] Ahmed, A. M.; Minallah, N.; Ahmed, N.; Ahmed, A. M.; Fazal, N. Remote sensing based vegetation classificati on using machine learning algorithms. In 2019 International Conference on Advances in the Emerging Computi ng Technologies (AECT), pp. 1271-1276, IEEE. https://doi.org/10.1109/AECT47998.2020.9194217.
[49] Leigh, H. W.; Magruder, L. A. Using dual-wavelength, full-waveform airborne lidar for surface classification and vegetation characterization. Journal of Applied Remote Sensing 2016, 10(4), 045001.
[50] Tan, S., Development of a multiwavelength airborne polarimetric lidar for vegetation remote sensing, Doctoral dissertation, University of Nebraska-Lincoln, Lincoln, NE, USA, 2003.
[51] Tan, S.; Narayanan, R. M. Design and performance of a multiwavelength airborne polarimetric lidar for vegetation remote sensing. Applied Optics 2004, 43(11), 2360-2368.
[52] Tan S.; Narayanan, R. A multiwavelength airborne polarimetric lidar for vegetation remote sensing: instrumentation and preliminary test results. 2002 IEEE Geoscience and Remote Sensing Symposium, Vol. 5, pp. 2675 -2677.
[53] LeCun, Y.; Bengio, Y.; Hinton, G. Deep learning. Nature 2015. 521(7553), 436–444.
[54] Venkatesan, R.; Li, B. Convolutional Neural Networks in Visual Computing: A Concise Guide. 2017, CRC Press. ISBN 978-1-351-65032-8.
[55] Balas, V. E.; Kumar, R.; Srivastava, R. Recent Trends and Advances in Artificial Intelligence and Internet of Things. 2019, Springer Nature. ISBN 978-3-030-32644-9.